

Energy-dependent flavour ratios in neutrino telescopes from charm

Atri Bhattacharya,^a Rikard Enberg,^b Mary Hall Reno^c and Ina Sarcevic^{d,e}

^aSpace sciences, Technologies and Astrophysics Research (STAR) Institute, Université de Liège, Bât. B5a, 4000 Liège, Belgium

^bDepartment of Physics and Astronomy, Uppsala University, Box 516, 751 20 Uppsala, Sweden

^cDepartment of Physics and Astronomy, University of Iowa, Iowa City, IA 52242, USA

^dDepartment of Physics, University of Arizona, Tucson, AZ 85721, USA

^eDepartment of Astronomy and Steward Observatory, University of Arizona, Tucson, AZ 85721, USA

E-mail: A.Bhattacharya@uliege.be, rikard.enberg@physics.uu.se,
mary-hall-reno@uiowa.edu, ina@physics.arizona.edu

Abstract. The origin of the observed diffuse neutrino flux is not yet known. Studies of the relative flavour content of the neutrino flux detected at Earth can give information on the production mechanisms at the sources and on flavour mixing, complementary to measurements of the spectral index and normalization. Here we demonstrate the effects of neutrino fluxes with different spectral shapes and different initial flavour compositions dominating at different energies, and we study the sensitivity of future measurements with the IceCube Neutrino Observatory. Where one kind of flux gives way to another, this shows up as a non-trivial energy dependence in the flavour compositions. We explore this in the context of slow-jet supernovae and magnetar-driven supernovae—two examples of astrophysical sources where charm production may be effective. Using current best-fit neutrino mixing parameters and the projected 2040 IceCube uncertainties, we use event ratios of different event morphologies at IceCube to illustrate the possibilities of distinguishing the energy dependence of neutrino flavour ratios.

Contents

1	Introduction	1
2	Neutrino fluxes at source from charm	3
2.1	Slow-jet supernova sources	3
2.2	Magnetar-driven supernovae	5
2.3	Atmospheric neutrinos	5
2.4	Other high energy neutrino fluxes	6
3	The effect of neutrino oscillation on flavour compositions at Earth	7
3.1	Best-fit parameters and uncertainties	7
3.2	Flavour composition at Earth	7
4	Inferring flavour ratio changes from event-rate ratios of different morphologies	13
4.1	Analysis of cascade to track ratio using IceCube HESE 7.5yr data	16
5	Summary and conclusions	17

1 Introduction

Our understanding of high energy neutrinos at PeV energies and higher and their sources has been bolstered by the stream of data collected at the IceCube Neutrino Observatory (IC) [1] since 2011, first published in Refs. [2, 3]. Analyses of IceCube data have repeatedly confirmed the existence of neutrino fluxes higher than—and extending to energies beyond—atmospheric neutrinos [4–7]. Conventionally, one expects such highly energetic neutrinos to come from extra-galactic astrophysical sources such as Active Galactic Nuclei (AGNs) or Gamma-Ray Bursts (GRBs), where they are produced due to collisions of rapidly accelerated protons with protons or with the copious abundance of photons in such environments. Alternatively, beyond the Standard Model (BSM) mechanisms such as the decay or annihilation of very heavy PeV-scale dark matter, may be responsible for the production of ultra-high energy neutrinos (see, e.g., [8–12]).¹ Further, the total flux may be a combination of astrophysical and BSM neutrino fluxes with different relative normalisation. More data in the future, potentially aided by a bigger version of IceCube called IceCube-Gen2 [13], will be needed to effectively determine their origins precisely.

The extra-terrestrial neutrino flux at IceCube is inferred to be nominally consistent with a uniform power-law [4–7]:

$$E^2 \frac{d\Phi}{dE} = \Phi_0 E^{-\gamma+2}. \quad (1.1)$$

There are hints, albeit inconclusive, due to the low event statistics typical of high energy neutrino fluxes, of disagreements between inferences of the flux spectrum from different data samples. For example, analysis of high energy starting events (HESE) collected over 7.5 years points to a steeply

¹To clarify our notation, we use the term *ultra-high energy* neutrinos to refer to neutrinos with energies $E \geq 100$ TeV.

falling (or soft) spectrum, with the best-fit value of $\gamma = 2.88$ [6]. An analysis involving only through-going muons seen over 9.5 years points to a much harder spectrum, with $\gamma = 2.3$ [5]. Other analyses with different subsets of IceCube data find best-fit values for the spectral index lying between these extremes [4, 7]. Several solutions discussing how these discrepancies may be ameliorated have been suggested; one among them is to assume that, at the higher end of the spectrum, neutrino fluxes from choked jets may dominate [7, 14].

No matter their origins, a fraction of these neutrinos arrive at Earth after having traversed large cosmological distances. Along the way, the three flavours of neutrinos, ν_e , ν_μ , and ν_τ , oscillate amongst themselves leading to a redistribution of their relative flavour content by the time they are detected at Earth vis-à-vis at the source [15, 16]. Therefore, complementary to studies of the shape and normalisation of the total flux, analyses of the relative neutrino flavour content as they appear in the neutrino flux at Earth can throw light on the mechanism of their production at source and on the physics of flavour mixing during propagation [17–25]. The former helps to understand the source environment where these interactions take place while the latter may be able to pinpoint traces of BSM physics that influence neutrino oscillation (see [26] for a review and references therein).

The IceCube Neutrino Observatory, with its three-dimensional arrangement of photo-detectors distributed over a large volume, is capable of detecting different event morphologies arising from different neutrino flavours interacting with nucleons in rock/ice: (a) cascades with their starting vertex inside the instrumented volume, initiated either by charged-current deep-inelastic scattering (DIS) involving electron or low-energy tau neutrinos with nucleons (N), or by neutral-current DIS of any neutrino flavour; (b) tracks from charged-current interaction of a ν_μ and a nucleon; or, (c) at energies more than a PeV, tau neutrino specific signatures such as double bangs from $\nu_\tau N$ charged-current interactions shortly followed by τ decay.² This makes it the only operating neutrino detector that can measure individual flavour components in the incoming extra-galactic neutrino flux, within the limits defined by the above event morphologies. In the future, Baikal-GVD [27] and KM3NeT/ARCA [28], both currently being built, may also be able to measure the flavour composition of astrophysical fluxes.

Inferring neutrino flavour composition at the source from that obtained from cascade, track, and tau relative event rates at IceCube requires knowledge of the neutrino mixing parameters from precision neutrino oscillation experiments at Earth. Indeed the ever narrowing error bars on the measurements of mixing angles θ_{12} , θ_{13} , and θ_{23} at experiments like Super-Kamiokande [29], Sudbury Neutrino Observatory [30], Daya Bay [31], etc., have gone a long way towards improving the robustness of such inferences.

Using these inputs, several studies in the past have studied how to infer the flavour composition using relative event rates of cascade and track morphologies [20, 21, 32]. These typically assume that the flux composition remains unchanged across the entire range of ultra-high energies 10 TeV–10 PeV where IceCube sees data.

However, it may be the case that neutrino fluxes originating from fundamentally different interactions—and thus with different spectral shapes and different initial flavour compositions—dominate at different energy ranges. If two or more competing fluxes indeed have different overall shapes and initial flavour compositions between 10 TeV and 10 PeV, the transition from one flux to

²At low energies below $\lesssim 1$ PeV these are difficult to distinguish from ν_e charged-current cascades owing to the τ decay happening very close to the initial $\nu_\tau N$ interaction.

another will induce an energy dependence in the flavour compositions seen at IceCube. An analysis of flavour composition assuming an unchanged flux over the entire range of energy will have missed this transition.

In this work we explore the impact of such a possibility. As an example, we consider the case of diffuse neutrino fluxes from slow-jet supernova (SJS) sources, where under the right conditions, neutrino fluxes from pion and kaon decays, i.e., with an initial relative composition of $\nu_e + \bar{\nu}_e : \nu_\mu + \bar{\nu}_\mu : \nu_\tau + \bar{\nu}_\tau = \frac{1}{3} : \frac{2}{3} : 0$, dominate up to energies of about 100 TeV, giving way to neutrinos from decays of heavier charmed mesons, the latter produced with the flavour composition $\frac{1}{2} : \frac{1}{2} : 0$. We consider the case of magnetar-driven supernovae where a similar transition takes place at much higher energies $\sim 10^{10}$ GeV, with potential consequences for flavour composition studies at IceCube-Gen2 in the future. We also evaluate an example in which the ultrahigh-energy neutrino flux comes from a mix of π/K and charm decays to neutrinos in sources.

We note that energy-dependent flavour composition transitions may also be caused by exotic Beyond Standard Model (BSM) physics effects such as neutrino decay or Lorentz invariance violation acting during neutrino propagation (see Refs. [33] and [26] for recent reviews and references therein). Some of these BSM effects may end up enforcing flavour ratio transitions similar, at least qualitatively, to those coming from the dominance of charm decay initiated neutrino fluxes at higher energies (as discussed in this work). This would make it difficult to disentangle the different underlying mechanisms. However, a full analysis involving such BSM effects is beyond the scope of this work.

The next section describes the two astrophysical sources of fluxes of neutrinos from charm. Section 3 reviews the effect of neutrino oscillations on flavour compositions at Earth, given source flavour ratios, as a function of energy. Our analysis of event-rate ratios based on event morphologies from different neutrino flavour induced events in IceCube is described in Section 4. Our summary and conclusions appear in Section 5.

2 Neutrino fluxes at source from charm

In this section, we provide a brief description of the different sources of neutrino fluxes we consider for our case studies. We refer to Refs. [14, 34, 35] for detailed descriptions of the models that we use.

We consider two main sources of neutrinos: slow-jet supernovae (SJS) and magnetar-driven supernovae (MdSn), which have in common that they yield a contribution of neutrinos produced from decays of charm quarks, which has both a different flavour composition and a different energy dependence than the conventional neutrinos produced from decays of pions and kaons. We stress that these are two examples of such sources that we use as simple models to point out the possible mechanism, but there may be other types of sources with other energy dependencies that give this effect too.

2.1 Slow-jet supernova sources

We first consider slow-jet supernovae (SJS) [37–39], where the neutrino flux is generated in a relativistic jet launched by a core-collapse supernova. The neutrino generation mechanism is similar to the standard scenario for gamma-ray bursts [40]: Protons are accelerated by Fermi acceleration in the jet and collide with ambient photons, and neutrinos are generated from decays of pions and kaons produced in the $p\gamma$ collisions, provided that the centre-of-mass energy exceeds the threshold for Δ^+

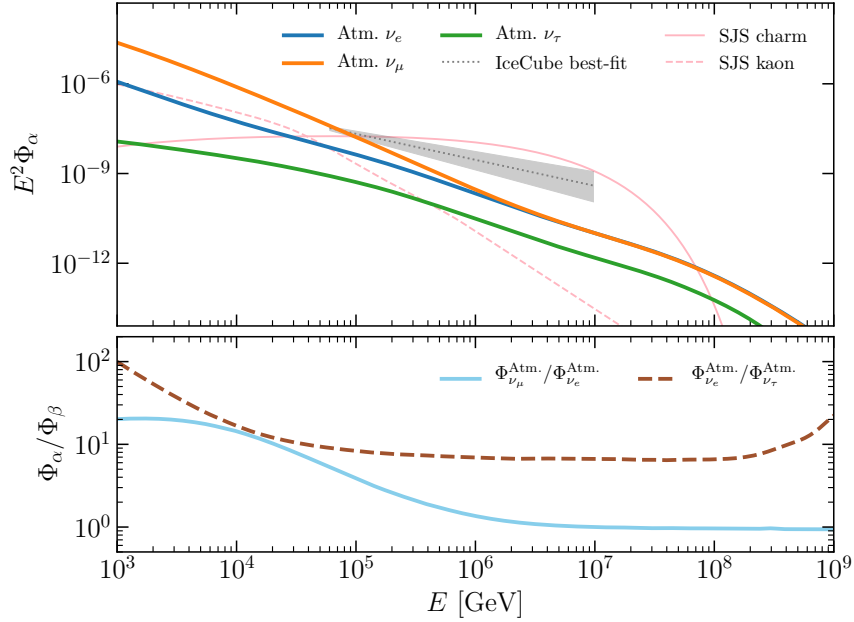


Figure 1. Angle averaged atmospheric neutrino fluxes [36] used to compute flavour ratio variations in Figs. 4, 5 and 8. Also shown are SJS charm and kaon diffuse $\nu_\mu + \bar{\nu}_\mu$ fluxes from Ref. [14] as used in this work, as is the best-fit uniform power-law flux (per flavour) inferred from 7.5-yr high-energy starting events data at IceCube [6]. The bottom panel shows the non-trivial flavour ratios, unrelated to neutrino oscillation, for the atmospheric fluxes as a function of energy.

production. Moreover, in a GRB the jet is ultra-relativistic and emits a burst of gammas generated by synchrotron radiation and inverse Compton scattering.

In contrast, the jet in an SJS is mildly relativistic. It is choked and stalls before it punches through the envelope, so there is no accompanying gamma ray burst, but there will be a visible optical supernova. But because of the different environment with a larger optical depth, in an SJS there may additionally be pp collisions that produce pairs of charm quarks, which, when they decay, give rise to an additional component of the neutrino flux. The relative sizes of the pp and $p\gamma$ components depend on the characteristics of the astrophysical environment (see also [41]).

The pp production of charm quarks has another important consequence. Pions and kaons are long-lived and will undergo both hadronic and radiative energy losses, or cooling, before decaying, so that the neutrino energies are downgraded. However, for the charmed hadrons (D mesons and Λ_c baryons) that are produced when the charm quarks hadronise, there are two factors to contribute to making them have much less cooling: First, they are very short-lived and decay before they interact to lose energy from hadronic cooling. Second, the efficiency of radiative cooling scales as $(\text{mass})^{-4}$, meaning that the heavier charmed hadrons are cooled less than pions and kaons.

On the other hand the production cross section for charmed hadrons is several orders of magnitude smaller than the cross section for pions and kaons, but in the competition between production and cooling it turns out that neutrinos from charm decays may dominate the neutrino flux at high energies. The cross-over energy where this happens depends on the detailed properties of the astrophysical source and the maximum energy of accelerated protons in the jet. For example, it turns out

that in AGNs, the cross-over energy is at a higher energy than the maximum proton energy making this effect non-existent, but in SJS it may be an important effect [34].

In Refs. [14, 34] we demonstrated that for realistic SJS properties there may be an appreciable component of neutrinos from charm decay that may be an important contribution to the diffuse flux detected by the IceCube neutrino observatory. In [42] it was further argued that IceCube-Gen2 has capabilities to detect SJS sources out to megaparsec distances.

2.2 Magnetar-driven supernovae

Magnetars are strongly magnetised, fast-rotating neutron stars that are expected to be sources of high energy neutrinos. Cosmic rays are likely accelerated to ultra-high energies by magnetic dissipation of the spindown energy in the magnetar, and do not escape the supernova ejecta, but rather produce charged pions through pp and/or $p\gamma$ interactions, which then decay to high-energy neutrinos. In Ref. [35], only the pp interactions are included since they dominate. In addition to pion production and decay, there are kaons and charmed hadrons that are produced that decay into neutrinos. As for SJS, neutrino production from charm is often neglected but can become the dominant contribution to the neutrino flux at early times when pions and kaons experience significant cooling before they decay. In magnetars, this significant cooling due to interactions of pions and kaons with the surrounding protons and photons happens for energies above 10^9 GeV. Thus for these energies, prompt decays of charm hadrons can be dominant source of very high energy neutrino production.

In Ref. [35], the neutrino fluence was evaluated for magnetar-driven supernovae (MdSn) and for magnetar-driven merger novae. In the former case, the supernova ejecta mass was taken to be between 10 and 35 solar masses (M_\odot), and the nucleon density was assumed to be homogeneous. For the latter case, when the rapidly rotating magnetars are born at the merger of the low-mass neutron star binaries, ejecta masses are taken to be between $10^{-2}M_\odot$ and $10^{-1}M_\odot$. While the charm contribution is not dominant over the full energy range, charm becomes significant for energies above $\sim 10^9$ GeV at the beginning of the burst. Late time emission is dominated by pion and kaon contributions.

Magnetar-driven supernovae with a magnetic field $B = 10^{14.5}$ G, an initial angular frequency of 10^{-4} s and the rate of $500 \text{ yr}^{-1} \text{ Gpc}^{-3}$ have pion dominated neutrino fluxes for energies up to $\sim 4 \times 10^9$ GeV, at which point kaon decays into neutrinos become important until $E_\nu \sim 10^{10}$ GeV when charm takes over [35]. The flavour ratio can be extracted from these fluxes as a function of energy. The overall uncertainty in the prediction of the neutrino flux from charmed meson decay is about an order of magnitude. Here, we use the central values of the prediction of the neutrino flux from charm.

2.3 Atmospheric neutrinos

An additional component of the detected neutrino flux, which is a background to the sources discussed above, is the atmospheric neutrino flux. Interactions of cosmic rays with the Earth atmosphere produce pions, kaons and charmed mesons. These mesons decay and produce neutrinos; pions and kaons give muon and electron neutrinos and antineutrinos, and secondary neutrinos are produced from muon decays, where muons come from pions and kaons. On the other hand, charmed mesons decay into all three flavours of neutrinos, thus producing ν_τ neutrinos, albeit to a lesser extent than ν_e and ν_μ [43, 44]. A direct flux of $\nu_\tau + \bar{\nu}_\tau$ cannot come from pion and kaon decays. The atmospheric

neutrino flux has been measured up to energies of several PeV by IceCube, currently without evidence for prompt neutrinos.

We compute the total atmospheric neutrino flux for each of the three flavours using MCEq [36], including both the conventional component from pions and kaons and the prompt component from charm. The former is computed based on Hillas-Gaisser’s 2012 H3a cosmic-ray model [45] and the SIBYLL-2.3c hadronic interaction model [46], while the latter is based on Ref. [47]. In Fig. 1 we show the angle averaged atmospheric flux for different flavours, as well as the diffuse neutrino flux from slow jet supernovae. The IceCube best fit for high energy neutrinos from ref. [6] sits only slightly below the predicted SJS neutrinos from charm. The lower plot shows that at higher energies, above a PeV, the atmospheric ν_e flux becomes identical to the ν_μ flux, both about an order of magnitude bigger than the ν_τ component. The equality of the ν_e and ν_μ flux for $E \gtrsim 10^7$ GeV is a consequence of the charm contribution becoming more important at higher energies.

High energy atmospheric ν fluxes are not affected by neutrino oscillation, as these travel relatively short distances (up to the diameter of the Earth) before they are detected; their relative compositions are determined solely by the underlying production mechanism. This is in contrast to low energy atmospheric neutrinos. In their traverse of as much as the Earth’s diameter through rock, the three flavours oscillate [48]. Indeed, such neutrinos are used by experiments such as Super-Kamiokande to determine oscillation parameters [29].

2.4 Other high energy neutrino fluxes

The cut-off in the cosmic ray spectrum at cosmic ray energies of ~ 50 EeV could be a signal of Greisen-Zatsepin-Kuzmin (GZK) effect [49, 50] in which the cosmic ray-photon interaction is above the threshold for Δ^+ production. Whether or not this is the GZK effect or a signal of the limits of cosmic accelerators, cosmic ray interactions with the cosmic background photons will produce a diffuse flux of ultra-high energy neutrinos [51–60]. With the GZK effect, this cosmogenic neutrino flux has primarily $\bar{\nu}_e$ that come from neutron decays for $E_\nu \lesssim 100$ PeV, while at higher energies, the initial flavour ratios are $\frac{1}{3} : \frac{2}{3} : 0$ characteristic of pion production and decay, along with secondary muon decays. While there is an interesting evolution of flavour ratios as a function of energy in the cosmogenic neutrino flux, charm production is unlikely to be a feature in the flavour composition of cosmogenic neutrinos since the cosmic ray-photon cross section for charm-pair production is significantly smaller than for Δ production [61].

Beyond Standard Model physics at the source could, in principle, involve charm production and decays, for example in the case of super-heavy dark matter annihilation to charm pairs (see, e.g., [62–65]). This annihilation channel could give interesting neutrino flavour signatures. A complication in the neutrino flavour ratios as a function of energy is that the charm states produced are highly virtual, so they will shower, hadronise and decay [66]. Different from charm production in sources, the dark matter annihilation essentially occurs in vacuum, so cooling processes do not come into play and all of the hadrons decay. The energy dependent neutrino flavour composition of the resulting neutrino flux is beyond the scope of the present work.

3 The effect of neutrino oscillation on flavour compositions at Earth

When neutrinos originate at distant, extra-galactic astrophysical sources such as GRBs, AGNs, SJS, etc., owing to the large distances the neutrinos subsequently propagate before reaching Earth, the oscillatory terms in the usual neutrino oscillation probability average out. As a consequence, the three flavours of neutrinos mix with each other incoherently with the probability [15, 16]:

$$P_{\nu_\alpha \rightarrow \nu_\beta} = \sum_{k=1,2,3} |U_{\alpha k}|^2 |U_{\beta k}|^2 \quad (3.1)$$

describing the transition of flavour ν_α to ν_β . Here, U_{ij} represents the ij -th element of the so-called PMNS matrix that describes the mixing between flavour and mass eigenstates of neutrinos [67]:

$$U_{\text{PMNS}} = \begin{bmatrix} 1 & 0 & 0 \\ 0 & c_{23} & s_{23} \\ 0 & -s_{23} & c_{23} \end{bmatrix} \begin{bmatrix} c_{13} & 0 & s_{13}e^{-i\delta_{\text{CP}}} \\ 0 & 1 & 0 \\ -s_{13}e^{i\delta_{\text{CP}}} & 0 & c_{13} \end{bmatrix} \begin{bmatrix} c_{12} & s_{12} & 0 \\ -s_{12} & c_{12} & 0 \\ 0 & 0 & 1 \end{bmatrix} \quad (3.2)$$

$$= \begin{bmatrix} c_{12}c_{13} & s_{12}c_{13} & s_{13}e^{-i\delta_{\text{CP}}} \\ -s_{12}c_{23} - c_{12}s_{23}s_{13}e^{i\delta_{\text{CP}}} & c_{12}c_{23} - s_{12}s_{23}s_{13}e^{i\delta_{\text{CP}}} & s_{23}c_{13} \\ s_{12}s_{23} - c_{12}c_{23}s_{13}e^{i\delta_{\text{CP}}} & -c_{12}s_{23} - s_{12}c_{23}s_{13}e^{i\delta_{\text{CP}}} & c_{23}c_{13} \end{bmatrix}. \quad (3.3)$$

where c_{ij} and s_{ij} are used to denote the $\cos(\theta_{ij})$ and $\sin(\theta_{ij})$ of the mixing angles θ_{ij} respectively. The CP-violating phase is represented as δ_{CP} .

The increasingly precise measurements of the neutrino mixing matrix are thanks to solar, atmospheric, and reactor neutrino data collected by dedicated neutrino detectors [29–31, 68–75]. In particular, recent studies of reactor neutrino data at Daya Bay [31], Double Chooz [69], and RENO [70] have significantly narrowed the uncertainties on the θ_{13} . Likewise, precision information on θ_{12} mainly comes from solar neutrino experiments, while atmospheric neutrino experiments and muon neutrino disappearance searches at Long Baseline experiments such as K2K [71], MINOS [72], T2K [73], and NO ν A [74] throw light on θ_{23} specifically. Finally, the CP violating phase δ_{CP} is only weakly constrained, primarily from T2K data [75].

Improved precision on these parameters, has in turn allowed us to understand interesting facets of neutrino phenomenology, including deviations from tri-bi-maximal mixing, the θ_{23} octant, and hints towards the true mass ordering.

3.1 Best-fit parameters and uncertainties

For our analysis, we use the most recent mixing parameters as tabulated in Nu-Fit [76, 77] obtained when using atmospheric SK data and assuming normal mass hierarchy. We find no tangible change in results when using best-fit parameters obtained assuming inverted hierarchy instead.

The 2040 projections on parameter uncertainties are obtained from Refs. [31, 78–80], and listed in Table 1 (see also Ref. [81]). In the analysis below, we assume that the best-fit values of these parameters remain the same as in current data.

3.2 Flavour composition at Earth

Using the values of the mixing matrix parameters as determined at neutrino oscillation experiments at Earth, it becomes straightforward to use equation 3.1 to compute the flavour composition of the

Parameter	Current Best-fit	2040 uncertainty (\pm)
$\sin^2 \theta_{13}$	$0.0223^{+0.0017}_{-0.0018}$	0.0018 [31]
$\sin^2 \theta_{12}$	$0.303^{+0.0338}_{-0.0330}$	0.005 [78]
$\sin^2 \theta_{23}$	$0.451^{+0.153}_{-0.042}$	0.018 [79]
δ_{CP}	$232^\circ^{+118}_{-88}$	35° [80]

Table 1. Oscillation parameters relevant to UHE flavour mixing and their current and 2040 projected 3σ uncertainties. Note that the 2040 projected 3σ uncertainty on θ_{23} has been scaled up from the 1σ data specified in Ref. [79], and should be considered approximate.

neutrino flux at Earth, Φ_α , given an initial composition at source.

To quantify the flavour composition of the neutrino flux at Earth, we look at different measures:

- flavour fractions defined as

$$f_\alpha = \frac{\Phi_\alpha}{\Phi_{\text{total}}} = \frac{\Phi_\alpha}{\sum_\beta \Phi_\beta}, \quad (3.4)$$

where the subscripts represent neutrino flavours and the sum over β runs over all three to give the total flux;

- flavour ratios between the fluxes of any two flavours ν_α and ν_β of the three comprising the total flux, defined as

$$r_{\alpha\beta} = \frac{\Phi_\alpha}{\Phi_\beta} = \frac{f_\alpha}{f_\beta}, \quad (3.5)$$

- and finally, ratios of cascades to μ -tracks and high-energy ν_τ double bangs, considered in a later section.

For each measure, the best-fit values of PMNS mixing matrix parameters give us the central values, while the corresponding upper and lower limits are obtained by varying oscillation parameters within their allowed 3σ ranges, and determining the relevant maxima and minima respectively.

For a flux with its origins in heavy quark decays that starts with $\frac{1}{2} : \frac{1}{2} : 0$ at the source ($(\frac{1}{2} : \frac{1}{2} : 0)$ -origin), we find that neutrino flavour mixing during propagation results in a composition at Earth, including mixing parameter uncertainties, of $(0.39 \pm 0.04 : 0.31 \pm 0.01 : 0.30^{+0.03}_{-0.04})_\oplus$. For comparison, for a flux at the source with a normalised flavour composition of $\frac{1}{3} : \frac{2}{3} : 0$ (e.g. from pion decay), it is well-known that the best-fit flavour fractions at Earth are nearly $\frac{1}{3} : \frac{1}{3} : \frac{1}{3}$, or more precisely $(0.33 \pm 0.04 : 0.34^{+0.03}_{-0.02} : 0.33^{+0.02}_{-0.03})_\oplus$.

In Fig. 2, we demonstrate these results for the three flavour fractions, including their variation due to current mixing matrix parameter uncertainties. With current uncertainties, resolving the two different flavour compositions considered here is a challenging prospect for any experiment. On the other hand, with future measurements of these parameters at dedicated neutrino oscillation experiments constraining them more stringently, distinguishing between individual flavour fractions may potentially become feasible by the year 2040.

An alternative way to demonstrate the flavour composition variation at Earth given an initial composition at source is in terms of the flavour fraction triangle as shown Fig. 3. Thus, given a normalised flavour composition of $\frac{1}{2} : \frac{1}{2} : 0$ at source, the red patch therein shows potential flavour

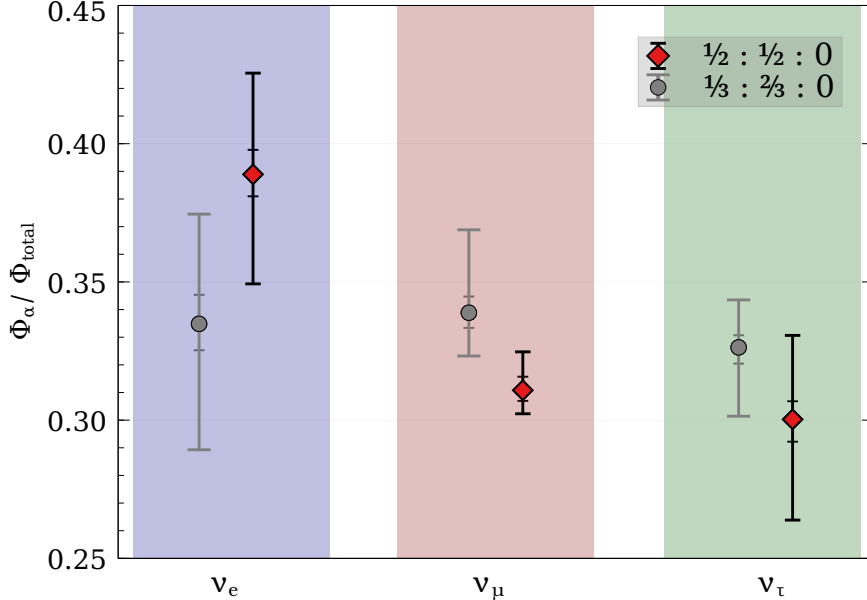


Figure 2. Flavour compositions as fraction of total flux at Earth for best fit mixing parameters and 3σ variation thereof. The smaller uncertainties are obtained using projected 2040 uncertainties on the underlying mixing parameters, with results especially from JUNO constraining $\sin^2(\theta_{12})$ [78, 82] while results from Hyper-Kamiokande [79] and DUNE [80] do the same to θ_{23} and to a lesser extent to δ_{CP} .

fractions at Earth for all possible variations of the mixing matrix parameters within their current 3σ uncertainties. This contrasts with the cyan patch which is similarly computed for a starting composition of $\frac{1}{3} : \frac{2}{3} : 0$.

Translated into flavour fraction ratios at Earth, we find that the $\Phi_{\nu_e}/\Phi_{\nu_\mu}$ ratio is ≈ 1.25 for a starting composition of $\frac{1}{2} : \frac{1}{2} : 0$ as opposed to 0.99 for a $\frac{1}{3} : \frac{2}{3} : 0$ initial flux. Concomitantly, the ν_τ/ν_e flavour ratio changes from 0.77 to 0.98, while, on the contrary, the ν_μ/ν_τ ratio remains largely unchanged.

Where two fluxes with different starting flavour compositions dominate at different energies, such transitions in the flavour ratios will be seen to occur at a specific energy. Specifically, for the case of SJS sources described previously, neutrinos from kaon-decays comprise the dominant component of flux up to energies of ~ 100 TeV and those from decays of charmed mesons likewise at higher energies; one therefore expects to find the ν_e/ν_μ flavour ratio to show a transition from 0.99 to 1.25 close to these energies. We may therefore define an energy dependent ratio between any two flavour components (say, α and β) of the total neutrino flux across the entire energy range as

$$\mathcal{F}_{\alpha\beta}(E_\nu) = \frac{\sum_i \Phi_\alpha^i(E_\nu)}{\sum_i \Phi_\beta^i(E_\nu)}, \quad (3.6)$$

where the summation over i iterates over fluxes *at Earth* from every relevant source. For example, in the SJS case, this summation would include the atmospheric neutrino flux of the specified flavour and fluxes from SJS due to kaon and charmed meson decays. As shown in Fig. 1, the dominant component of the flux changes over the energy range, in this case, from atmospheric neutrinos up to tens of TeV,

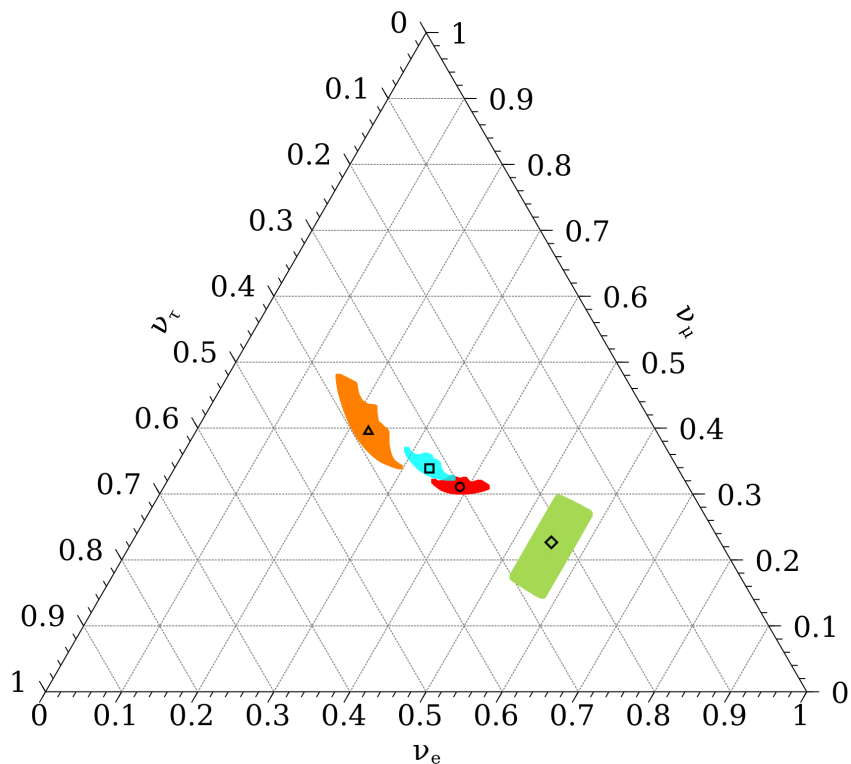


Figure 3. Flavour fractions at Earth for best-fit and current 3σ variation of mixing matrix parameters computed with various initial flux fractions. The red patch with \circ showing the best-fit point is for a starting flavour composition of $\frac{1}{2} : \frac{1}{2} : 0$ (charmed meson decays, this work, and **see also** [83]), while the cyan patch with \square as best-fit point is computed assuming a starting flux of $\frac{1}{3} : \frac{2}{3} : 0$ [22]. The green patch (\diamond) and orange (\triangle) patches assume neutrino fluxes originating from from neutron decays (initial composition $1 : 0 : 0$, for example for cosmogenic fluxes) and muon-damped sources ($0 : 1 : 0$ starting flavour) respectively [22].

to those from kaon decays at SJS up to 100 TeV, and finally to the flux from charmed meson decays. This induces a non-trivial energy-dependence on the flavour ratios as shown in Fig. 4. However, the dominance of the atmospheric neutrino flux over both components of the SJS flux up to energies of several tens of TeV, alters the picture significantly. Since this flux is dominantly comprised of muon neutrinos at low energies (see Fig. 1), we find that the ν_e/ν_μ flavour ratio drops steeply at energies below ~ 50 – 60 TeV until it falls to about 0.05 at 1 TeV. Conversely, the rise of this ratio with energy, first to ≈ 1 at energies of around 250 TeV, where the atmospheric neutrino flux is all but gone, and thereafter to 1.25 at higher energies is markedly steeper than it would be were the transition to solely involve the two SJS fluxes.

Similar conclusions may also be drawn for the ν_τ/ν_e flavour ratio, which, in the absence of atmospheric neutrino fluxes, should drop from a value of 0.975 at the lower energies, up to 100 TeV, to 0.772 thereafter. However, in this case, the dominance of atmospheric neutrino fluxes — with very little ν_τ content — at lower energies completely changes the nature of this transition: the ν_τ/ν_e flavour ratio rises, instead of falling, from lower to higher energies until, at around a PeV, it reaches a

value of 0.772 at ~ 1 PeV marking the beginning of the dominance of the neutrino flux from charmed meson decays. We show these results, including the uncertainties associated with the flavour ratios, in Fig. 4 for SJS sources (top panel).

For MdSn sources, similar transitions appear at much higher energies ~ 10 EeV, making the consideration of atmospheric neutrino fluxes moot. The flavour ratio as described in equation 3.6, therefore, only involves astrophysical fluxes. We show these results in the bottom panel of Fig. 4.

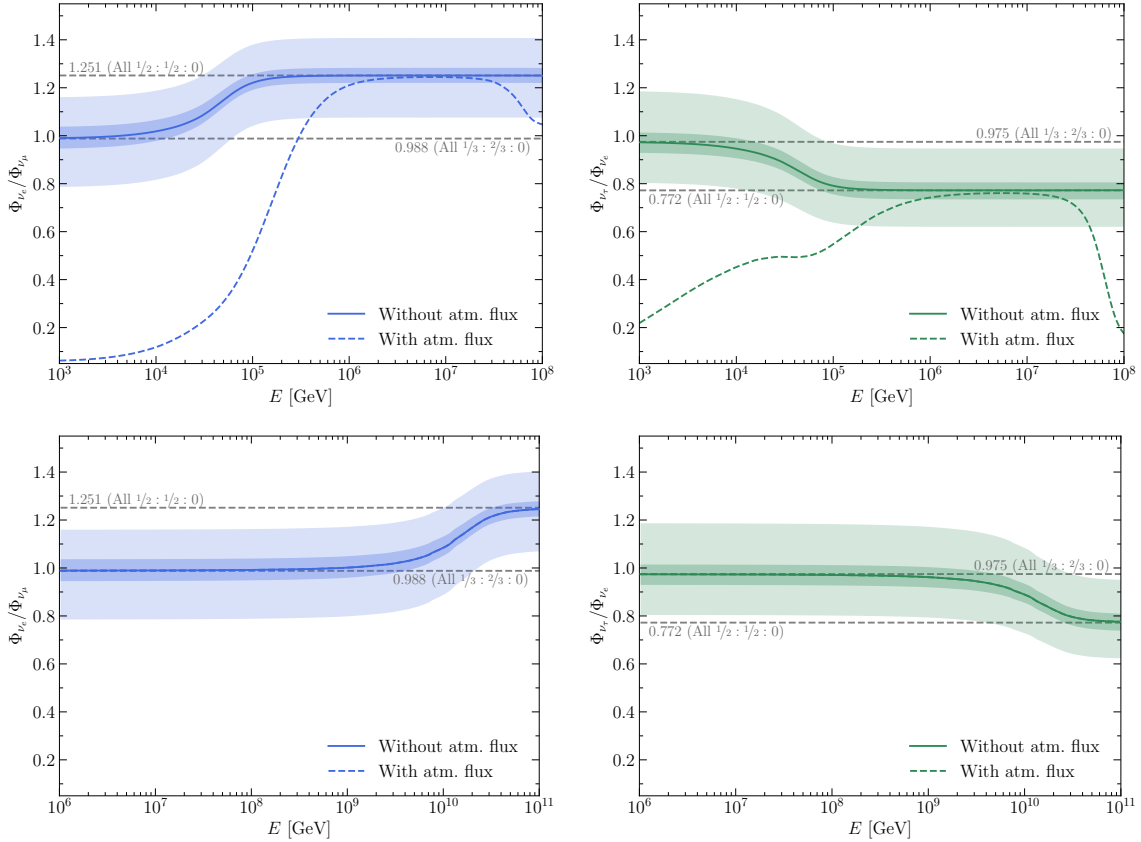


Figure 4. Energy dependent flavour ratios at Earth for our sample SJS (MdSn) source shown in the top (bottom) panel. Uncertainty bands are computed using current 3σ ranges of the mixing matrix parameters deduced while including SK atmospheric data [76]. Narrower uncertainty bands are derived assuming reduced uncertainties on mixing parameters projected by the year 2040. For SJS sources, the dip in the ratios seen at high energies $\gtrsim 30$ PeV is due to the source flux dropping exponentially beyond a few PeV and quickly falling below atmospheric flux levels (see Fig. 1).

With our choices of parameters for the population of SJS, we find that the charm-origin neutrino flux completely dominates over other flux components between 1–10 PeV energies, however, more realistic scenarios may lead to fluxes from SJS that constitute only a fraction of the total flux admixture, with the remainder coming from π/K decays. Current uncertainties in the neutrino mixing parameters preclude the possibility of disentangling a fully $(\frac{1}{2} : \frac{1}{2} : 0)$ -origin flux from a fully $(\frac{1}{3} : \frac{2}{3} : 0)$ -origin flux. By contrast, the significant reduction in uncertainties projected by 2040 offer hope of detecting similar flavour ratio transitions. It also raises the question as to what fraction of the total flux reaching Earth needs to be of a charm origin — assuming the remaining flux to originate

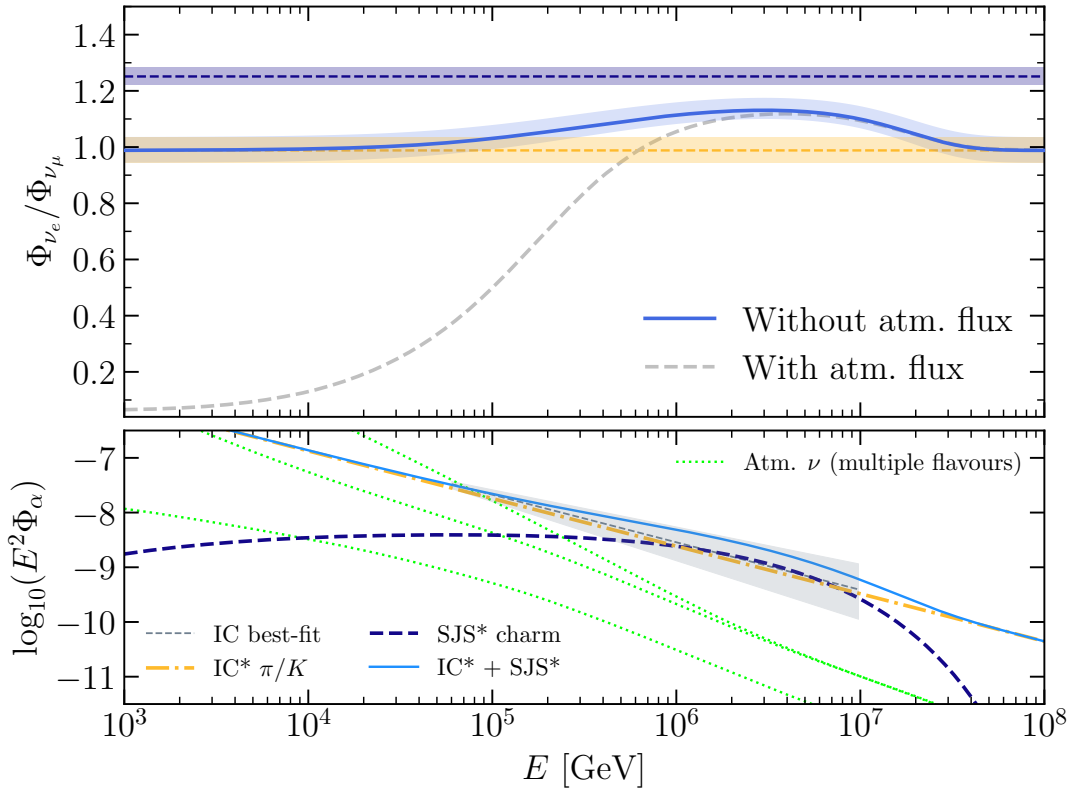


Figure 5. Top: The $\Phi_{\nu_e}/\Phi_{\nu_\mu}$ flavour ratio (solid blue curve) as a function of energy for the combined power-law and SJS-charm flux shown in the lower panel, without the angle-averaged atmospheric neutrino flux contribution. The dashed grey line includes the atmospheric neutrino flux. For comparison, flavour ratios corresponding to a fully $(\frac{1}{3} : \frac{2}{3} : 0)$ -origin flux (light orange) and fully $(\frac{1}{2} : \frac{1}{2} : 0)$ -origin flux (purple) are shown along with their 3σ maximum and minimum ranges allowed by the projected 2040 uncertainties of mixing parameters. **Bottom:** The different fluxes used in this analysis. Fluxes labelled with an ‘*’ have been rescaled as described in the text. For comparison, the unscaled central value of the IceCube HESE best-fit single power law curve is shown with grey dashes, along with its uncertainty band in grey. The total flux comprising the rescaled power-law and the SJS-charm flux lies within the uncertainty band corresponding to the IceCube best-fit power-law flux between the energies of 60 TeV–10 PeV. The three flavours of atmospheric neutrinos are shown as light green dotted curves.

with a $\frac{1}{3} : \frac{2}{3} : 0$ composition — to make the transition discernible accounting for the 2040 mixing parameter uncertainties.³ To understand this, we analyse a hypothetical scenario in which the flux from SJS is reduced by a constant factor and combined with the IceCube single power-law flux. With the power-law flux normalized to 85% of the best-fit value, labelled as IC*, still within the IceCube uncertainty band of the flux normalization [6], the SJS neutrino spectrum is normalized (labelled as SJS*) such that at neutrino energy of 1 PeV, the SJS* and IC* are equal. The combined flux lies within the uncertainty band corresponding to the IceCube best-fit power-law flux between energies of 60 TeV–10 PeV, as shown in the lower panel of Fig. 5. Assuming the IceCube power-law spectrum comes fully from π/K -origins, practically, this implies that the charm-origin flux component in the total flux would be 50%. We use this total flux to investigate how the flavour ratios change as a

³In practice, any detectability would depend on the event statistics and therefore hinge critically on the energy where the transition starts.

function of energy. In particular we show the $\Phi_{\nu_e}/\Phi_{\nu_\mu}$ flavour ratio in the upper panel of Fig. 5. We note that while the maximum flavour ratio in this scenario does not rise to a value of 1.251 representative of a dominant charm-origin flux, the central value grows gradually to a maximum of about 1.131 (1.119 when including atmospheric neutrino fluxes in the total flux) — higher than the maximum value of the ratio for a fully $(\frac{1}{3} : \frac{2}{3} : 0)$ -origin flux allowed by the 3σ projected 2040 uncertainty ranges of mixing parameters. The rise becomes tangible at energies between 300–400 TeV.

4 Inferring flavour ratio changes from event-rate ratios of different morphologies

Events originating from neutrino-nucleon ($\nu_\alpha N$) interactions, where the subscript α refers to any of the three neutrino flavours, occurring within IceCube’s instrumented volume may be classed into different groups based on their morphologies that depend on the initiating neutrino flavour and the mediating boson:

1. Z^0 -boson mediated neutral current event initiated by any flavour produce cascades, with a final state neutrino carrying away energy from the interaction without detection by the detector. For these events, the energy deposited in the detector, E_{dep} , is substantially different from the energy of the initial neutrino E_ν .
2. Charged current events initiated by $\nu_e N \rightarrow e^- X$ interactions are detected as nearly-spherical cascades in the detector. As opposed to neutral current events, the entire energy from the incoming ν_e is deposited in the cascade with the outgoing e^- almost immediately losing its energy as well; thus, in this case we can assume $E_{\text{dep}} = E_\nu$.
3. On the contrary, a charged current event from $\nu_\mu N \rightarrow \nu^- X$ produces a cascade, with substantial energy taken away by the final state muon. As the muon scatters away from the interaction, it loses energy predominantly via bremsstrahlung, with the resulting track-like event topology a signature of a ν_μ initiated event.
4. Charged current events initiated by $\nu_\tau N$ interactions also show up as cascades; however, the outgoing τ^- shows up as a faint track that traverses a short distance before it decays producing a secondary cascade or “bang”. If both cascades are detected within the detector’s instrumented volume but separated by enough distance to allow the cascades to be individually resolved, this “double-bang” becomes a smoking gun signature of a charged current ν_τ event.

With long-lived tracks being exclusive to ν_μ initiated events, estimates of the cascade to track event rate ratios [22] across the entire HESE-sensitive span of energies will throw light on the relative ν_μ content in the neutrino flux arriving at Earth. In turn, any change in this quantity would directly point to changes in the flavour content of the dominant flux between 10 TeV and 10 PeV. Having already computed the final flavour composition at Earth for both pion/kaon-dominated initial fluxes (flavour fraction $\frac{1}{3} : \frac{2}{3} : 0$ at source) and heavy meson dominated initial flux ($\frac{1}{2} : \frac{1}{2} : 0$ initial flavour composition), we can translate these results into event ratios between different morphologies by making use of deeply inelastic νN scattering cross-sections in the literature [84].

In Fig. 6, we show the best-fit cascade to track ratio for a neutrino flux originating with an initial composition of $\frac{1}{3} : \frac{2}{3} : 0$ and compare that with an initial composition of $1 : 1 : 0$. We find that for

a neutrino flux originating from charmed meson decays in the composition $\frac{1}{2} : \frac{1}{2} : 0$, the expected cascade-to-track event ratio is $3.61_{-0.19}^{+0.13}$, as opposed to $3.23_{-0.34}^{+0.20}$ for a $(\frac{1}{3} : \frac{2}{3} : 0)$ -origin flux (e.g., from pion decays). The uncertainties represent the maximum and minimum values of the ratios, obtained in each case by varying the mixing matrix parameters over their current 3σ range. With projected uncertainties in these parameters expected to be significantly reduced in the future, we find that cascade-to-track ratios will allow resolving the two different initial flux compositions at more than 3σ significance by the year 2040. Similarly, we find that at high energies, assuming the efficiency of resolving tau double bangs from other cascades becomes 100% efficient, the cascade to double bang ratio becomes $2.74_{-0.37}^{+0.49}$ for a flux with a $\frac{1}{2} : \frac{1}{2} : 0$ starting flavour composition, in contrast to $2.36_{-0.25}^{+0.32}$ for one starting with $\frac{1}{3} : \frac{2}{3} : 0$.

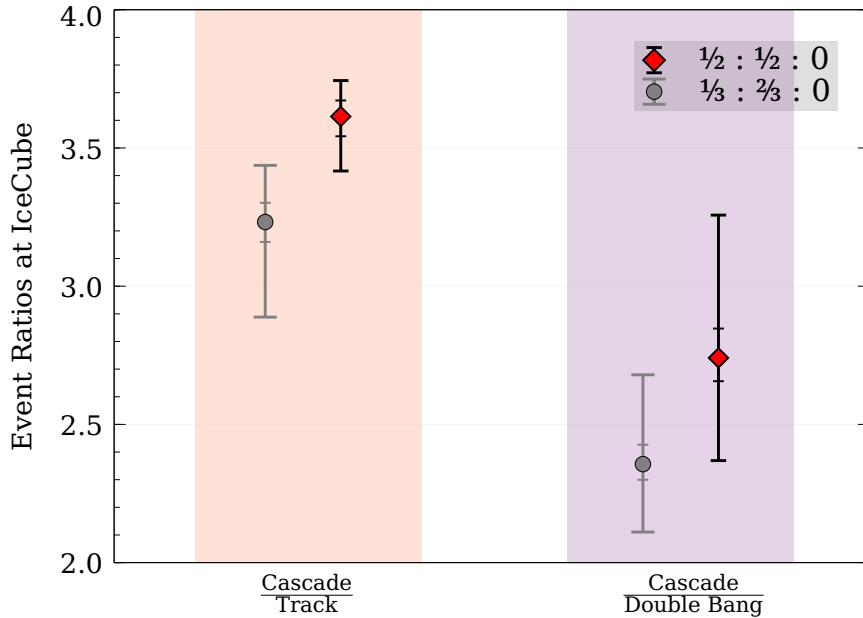


Figure 6. Cascade to track and cascade to double bang event ratios at Earth detectors for fluxes starting at $\frac{1}{2} : \frac{1}{2} : 0$ and $\frac{1}{3} : \frac{2}{3} : 0$ at the source. The evaluation is made at energies of 10 PeV, at and over which ν_τ signature events are expected to be distinguishable from general cascades. Error bars represent variation in the ratios due to 3σ uncertainties of mixing parameters, both current (bigger error bars) and projected for 2040 (smaller).

The transition from pion dominated to charm happens at a specific energy (depending on conditions in source). As we have seen in Fig. 4, this induces a non-trivial energy dependence in flavour ratios which directly carries over to cascade-to-track event ratios; additionally, the latter are also influenced by a mild E -dependence of the ratio of CC to NC cross-sections.

For ν_τ initiated events, the higher the energy of the initial ν_τ the longer the out-going τ track. Towards the lower-energy end of the HESE data, relatively short-lived tau tracks imply the final τ decay cascade cannot be resolved from the more catastrophic initial cascade which either completely or partially overlaps the former. For incoming ν_τ with super-PeV energies, on the other hand, the final tau becomes sufficiently long-lived that the two bangs can be distinguished from each other and τ double bangs become an exclusive class of events. Thus, while IceCube can distinguish between

cascades including double-bangs and tracks across the entire energy range, it is only weakly sensitive to tau-specific signatures at lower energies ($\lesssim 1$ PeV). As a consequence, double bang/cascade or double bang/track become useful only at high energies. However, this means that the transition in the flavour ratio needs to happen at energies beyond a PeV. This is not the case for SJS sources we consider but may work for other sources. As an example, for magnetars, the kaon-charm transition occurs at $\sim 10^{10}$ GeV [35], however poor statistics make it challenging to draw any conclusions.

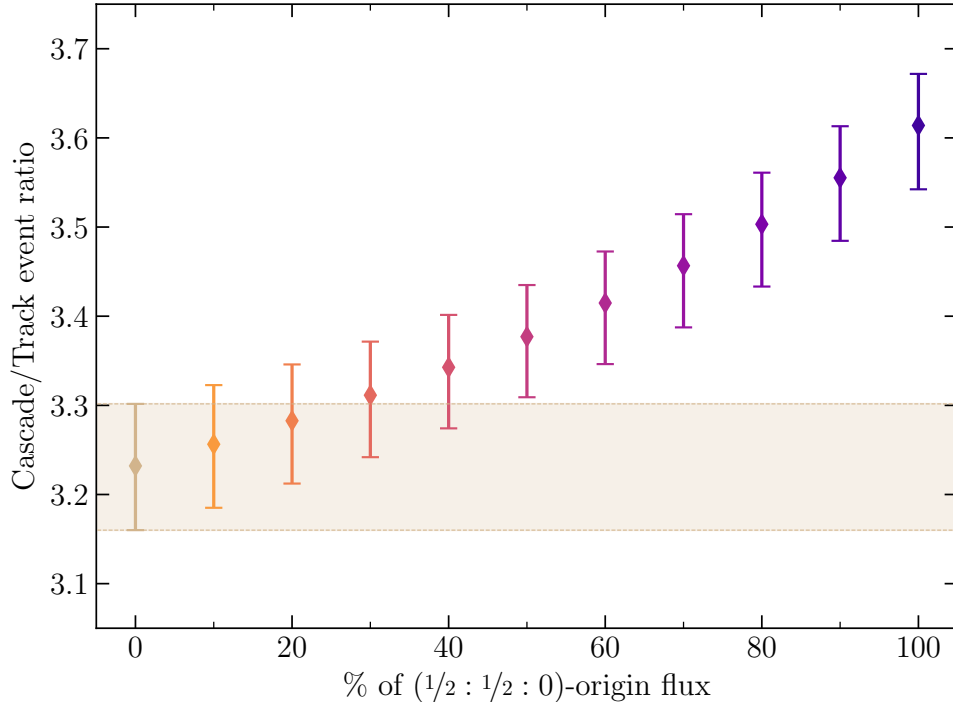


Figure 7. Cascade to track event ratios as a function of the percentage flux coming from charm-decay with the rest assumed to originate with a $\frac{1}{3} : \frac{2}{3} : 0$ composition. For each point, the error bars represent the uncertainty of the ratio for a full scan of the neutrino mixing parameters over their projected 2040 3σ uncertainties. We show this uncertainty band corresponding to the fully $\frac{1}{3} : \frac{2}{3} : 0$ flux extended across the entire x -axis (tan band) to illustrate what percentage of $\frac{1}{2} : \frac{1}{2} : 0$ flux in the admixture causes the ratio to become distinguishable from this band.

As discussed above, an admixture of neutrinos from π/K and an appropriately normalized SJS spectrum of neutrinos that is dominated by charm is consistent with IceCube measurements of the diffuse flux. To display the sensitivity of the cascade to track ratio to an admixture, in Fig. 7 we show the cascade to track event ratio as a function of the percentage of charm-origin flux in the admixture. As usual, the remainder is assumed to be composed entirely of neutrinos from $(\frac{1}{3} : \frac{2}{3} : 0)$ -origin. For each admixture, the upper and lower limits represent variation of the mixing parameters over their 3σ 2040 projected uncertainties. We find that at least a $\sim 50\%$ proportion of the neutrino flux needs to come from charm decays in the source to be discernible from neutrino sources dominated by π/K decays.

4.1 Analysis of cascade to track ratio using IceCube HESE 7.5yr data

In this section, we investigate if current data, notwithstanding the low statistics, show any trend of transition in flavour ratios within 10 TeV to 10 PeV. To this end, we make use of the IceCube HESE data-set collected over 7.5 years. To the extent that IceCube can clearly distinguish between cascades and μ -tracks, over the entire HESE energy range but can only distinguish double bangs from ν_e cascades at the higher energy end of the spectrum, for our analysis, we shall categorise double bangs and ν_e cascades together distinct from ν_μ CC tracks.

The HESE sampling comprises 102 events with E_{dep} measured between 10 TeV–2.1 PeV [6]. The lower-end of the spectrum ($E_{\text{dep}} \sim [10, 60]$ TeV) is dominated by atmospheric neutrino fluxes, despite the analysis involving significant background rejection. Instead, we focus on the 60 events with deposited energies above 60 TeV, allowing us to work with a pre-dominantly extra-galactic flux throughout.

While the data identifies each event with its E_{dep} and morphology, we need to “re-construct” the incoming neutrino energy for each. We do this using a simple Monte-Carlo analysis, whereby, out of the entire set of cascade events, we randomly categorise events as CC or NC based on the ratio of neutral-current to charged-current νN cross-sections. For the former, we assume $E_{\text{dep}} \approx E_\nu$; for the latter we scale the E_{dep} to get E_ν : $E_\nu = E_{\text{dep}} / \langle y(E_\nu) \rangle$, where y is the inelasticity of the interaction. At these energies, $\langle y(E) \rangle$ is slowly-varying, so we simplify the analysis by assuming $\langle y(E_\nu) \rangle \approx \langle y(E_{\text{dep}}) \rangle$. At the end of this exercise, we are left with a data-set of 60 events, with each identified with its initial neutrino energy E_ν and cascade or track morphology.

Since our goal is to determine flavour ratio transitions between low and high energies, we bin the events by their E_ν . To assign equivalent statistical weights to low and high energy bins, we split the set of events into two bins with an equal number of events (i.e. 30) in each. Note that, since event statistics worsens with increasing energies, binning in this manner leads to the bin widths being very unequal. We can now compute the ratio of the number of cascades and double bangs taken together to the number of muon-track events in each bin. To offset the randomness of classification of cascades into NC and CC events, we run the MC analysis over a million times and extract the mean ratios for the two bins. The results are shown in the left panel of Fig. 8, as compared with the flavour ratio transition expected for the case of SJS sources. We find that the IceCube ratio as evaluated here changes from 2.00 ± 1.24 for the lower energy bin to 3.39 ± 1.39 . The error bars on the ratios represent 1σ Poisson uncertainties around the mean values. We specifically emphasise that these uncertainties do not directly use or correlate to the uncertainties on neutrino mixing matrix parameters.

While the computed cascade-to-track ratios show hints of growth at higher energies, the associated uncertainties — a consequence of the inevitable low event statistics — are simply too large to allow a definitive conclusion whether there is a growth that points towards the dominance of a $(\frac{1}{2} : \frac{1}{2} : 0)$ -origin flux at the higher energies. Certainly, with current statistics, a 50 : 50 mix of π/K and charm sources at $E_\nu = 1$ PeV illustrated in Fig. 5 cannot be tested. More fine-grained binning would improve the energy resolution of the flavour transition; however this would be at the cost of even poorer per-bin statistics, in turn leading to even higher error bars on the final ratios. Nonetheless, we have checked that the trend of growth in the ratio persists even with finer binning, by using 3 (20 events / bin) and 4 bins (15 events / bin), although as mentioned before, it becomes progressively weaker with poorer per-bin event statistics. Low statistics of current PeV-scale and higher energy

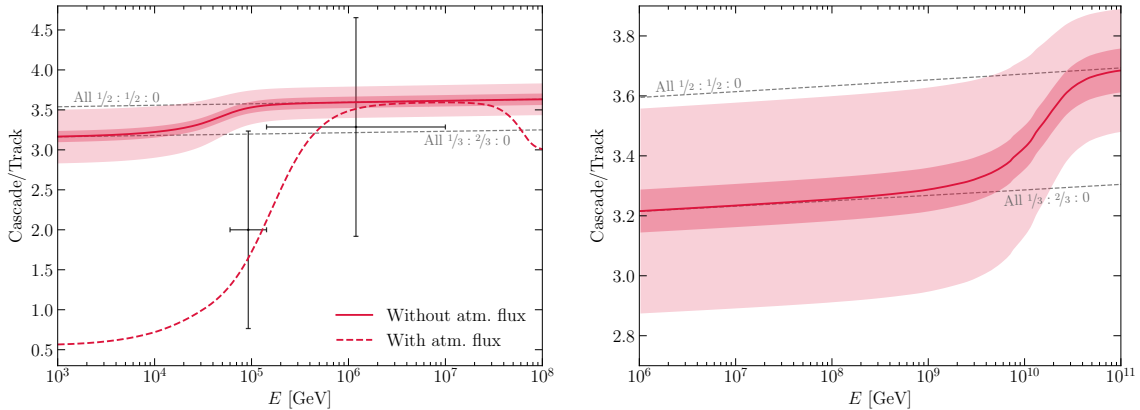


Figure 8. Left: Ratio of cascade to track events as a function of neutrino energy E assuming the extragalactic flux to originate at slow-jet sources. The steep drop off of the ratio at lower energies is due to the dominance of atmospheric neutrino fluxes. Also shown are the ratios inferred from IceCube HESE 7.5-yr data at two separate bins as described in the text. The grey error bars represent 1σ Poisson uncertainties on the mean value of the ratio for each bin. **Right:** Same as left, but for MdSn sources. Note that, since atmospheric fluxes play a negligible role at PeV energies and higher, we have omitted them from this plot, in contrast to the SJS plot on the left. In both figures, uncertainty bands are computed using 3σ uncertainty ranges of the current (light bands) and 2040 (darker bands) mixing matrix parameters.

data, with the HESE data containing only 3 events with deposited energies over a PeV, prohibit a similar analysis involving MdSn sources.

We note that the analysis presented in this section does not take into account experimental efficiencies in distinguishing between the different event morphologies, nor any particular experimental biases. It serves as a proof of principle for how similar analyses, potentially with refinements incorporating such considerations, may be carried out to determine energy-dependent flavour ratio variations in the future when more statistics will have accrued at IceCube or other neutrino telescopes.

5 Summary and conclusions

The many successes of IceCube since starting taking data in 2010 as an 86-string, 1 km^3 neutrino observatory have opened up an exciting window into the study of highly energetic astrophysical sources where high energy neutrinos originate and the propagation of these elusive particles. Understanding the flavour composition of the incoming neutrino flux is a key component towards understanding the nature of its source, complementary to and as important as understanding the overall spectral shape and magnitude thereof.

While the question of flavour fractions arriving at Earth has been discussed in the literature, such discussions have typically assumed starting flavour ratios of $\frac{1}{3} : \frac{2}{3} : 0$ from the decay of light mesons, or $1:0:0$ from neutron decay, or $0:1:0$ from muon damped sources. In this work, we have focused on charmed meson decay initiated neutrino fluxes that lead to a $\frac{1}{2} : \frac{1}{2} : 0$ distribution of flavours at source. Using current best-fits for neutrino mixing parameters, we have shown that standard flavour mixing reduces this to $0.39 : 0.31 : 0.30$ by the time the flux reaches Earth, as opposed to approximately $\frac{1}{3} : \frac{1}{3} : \frac{1}{3}$ at Earth for a $\frac{1}{3} : \frac{2}{3} : 0$ initial flavour composition. Using this result and uncertainties

associated with neutrino flavour mixing parameters, we have updated the corresponding patch in the flavour triangle, see Fig. 3.

We have discussed the implications for IceCube should the dominant neutrino flux differ in its flavour composition at lower (TeV) energies vis-à-vis at higher (PeV) energies. Within the realm of standard model physics, this could happen if neutrino production at source is predominantly from light meson decays at one edge of the spectrum, but from charmed and heavier mesons at the other. This would be the case for neutrino fluxes originating from slow-jet sources and magnetar-driven supernovae, for instance. For the former, we have shown that for very representative assumptions of source parameters, the transition in flavour composition may happen within the TeV-PeV energy range to which current IceCube data is sensitive. For the latter, a similar transition is expected at significantly higher energies (between 10^9 – 10^{11} GeV), with low event statistics at these energies making the transition significantly more challenging to detect. Radio detection of neutrinos [85] in this ultra-high energy range might be able contribute to flavour studies [86].

Knowing that the transition may be quantified in terms of flavour fraction ratios, and concretely seen in neutrino telescope experiments in terms of ratios of different event morphologies, we have used a sample of current IceCube data — HESE 7.5-yr — to look for any hints pointing to such transitions. The IceCube best-fit single power law with uncertainties permits a 50 : 50 admixture of a power law from π/K decays and a SJS charm contribution to the diffuse astrophysical neutrino flux. We find that the relatively low statistics of current events is insufficient to allow a conclusion about the flavour composition at sources, but we expect that the method used here, scaled up for data from IceCube-Gen2, will provide more definitive conclusions.

Acknowledgments

We thank M. Bustamante, C. Pérez de los Heros, C. Glaser and A. Hallgren for discussions. This work is supported in part by the U.S. Department of Energy Grant DE-SC-0010113 (MHR) and in part by the U.S. Department of Energy Grant DE-FG02-13ER41976/DE-SC-0009913 (IS).

References

- [1] ICECUBE collaboration, *Icecube - the next generation neutrino telescope at the south pole*, *Nucl. Phys. B Proc. Suppl.* **118** (2003) 388 [[astro-ph/0209556](#)].
- [2] ICECUBE collaboration, *First observation of PeV-energy neutrinos with IceCube*, *Phys. Rev. Lett.* **111** (2013) 021103 [[1304.5356](#)].
- [3] ICECUBE collaboration, *Evidence for High-Energy Extraterrestrial Neutrinos at the IceCube Detector*, *Science* **342** (2013) 1242856 [[1311.5238](#)].
- [4] ICECUBE collaboration, *Measurements using the inelasticity distribution of multi-TeV neutrino interactions in IceCube*, *Phys. Rev. D* **99** (2019) 032004 [[1808.07629](#)].
- [5] ICECUBE collaboration, *Measurement of the Diffuse Astrophysical Muon-Neutrino Spectrum with Ten Years of IceCube Data*, *PoS ICRC2019* (2020) 1017 [[1908.09551](#)].
- [6] ICECUBE collaboration, *The IceCube high-energy starting event sample: Description and flux characterization with 7.5 years of data*, *Phys. Rev. D* **104** (2021) 022002 [[2011.03545](#)].

- [7] ICECUBE collaboration, *Characteristics of the diffuse astrophysical electron and tau neutrino flux with six years of IceCube high energy cascade data*, *Phys. Rev. Lett.* **125** (2020) 121104 [[2001.09520](#)].
- [8] A. Bhattacharya, M.H. Reno and I. Sarcevic, *Reconciling neutrino flux from heavy dark matter decay and recent events at IceCube*, *JHEP* **06** (2014) 110 [[1403.1862](#)].
- [9] A. Bhattacharya, R. Gandhi and A. Gupta, *The Direct Detection of Boosted Dark Matter at High Energies and PeV events at IceCube*, *JCAP* **03** (2015) 027 [[1407.3280](#)].
- [10] M. Chianese, G. Miele and S. Morisi, *Interpreting IceCube 6-year HESE data as an evidence for hundred TeV decaying Dark Matter*, *Phys. Lett. B* **773** (2017) 591 [[1707.05241](#)].
- [11] M. Chianese, D.F.G. Fiorillo, G. Miele, S. Morisi and O. Pisanti, *Decaying dark matter at IceCube and its signature on High Energy gamma experiments*, *JCAP* **11** (2019) 046 [[1907.11222](#)].
- [12] B. Skrzypek, M. Chianese, C.A. Argüelles and C. Delgado Argüelles, *Multi-messenger high-energy signatures of decaying dark matter and the effect of background light*, *JCAP* **01** (2023) 037 [[2205.03416](#)].
- [13] ICECUBE-GEN2 collaboration, *IceCube-Gen2: the window to the extreme Universe*, *J. Phys. G* **48** (2021) 060501 [[2008.04323](#)].
- [14] A. Bhattacharya, R. Enberg, M.H. Reno and I. Sarcevic, *Charm decay in slow-jet supernovae as the origin of the IceCube ultra-high energy neutrino events*, *JCAP* **06** (2015) 034 [[1407.2985](#)].
- [15] J.G. Learned and S. Pakvasa, *Detecting tau-neutrino oscillations at PeV energies*, *Astropart. Phys.* **3** (1995) 267 [[hep-ph/9405296](#)].
- [16] S. Pakvasa, W. Rodejohann and T.J. Weiler, *Flavor Ratios of Astrophysical Neutrinos: Implications for Precision Measurements*, *JHEP* **02** (2008) 005 [[0711.4517](#)].
- [17] M. Kachelriess and R. Tomas, *High energy neutrino yields from astrophysical sources I: Weakly magnetized sources*, *Phys. Rev. D* **74** (2006) 063009 [[astro-ph/0606406](#)].
- [18] S. Choubey and W. Rodejohann, *Flavor Composition of UHE Neutrinos at Source and at Neutrino Telescopes*, *Phys. Rev. D* **80** (2009) 113006 [[0909.1219](#)].
- [19] S. Hummer, M. Maltoni, W. Winter and C. Yaguna, *Energy dependent neutrino flavor ratios from cosmic accelerators on the Hillas plot*, *Astropart. Phys.* **34** (2010) 205 [[1007.0006](#)].
- [20] O. Mena, S. Palomares-Ruiz and A.C. Vincent, *Flavor Composition of the High-Energy Neutrino Events in IceCube*, *Phys. Rev. Lett.* **113** (2014) 091103 [[1404.0017](#)].
- [21] M. Bustamante and M. Ahlers, *Inferring the flavor of high-energy astrophysical neutrinos at their sources*, *Phys. Rev. Lett.* **122** (2019) 241101 [[1901.10087](#)].
- [22] N. Song, S.W. Li, C.A. Argüelles, M. Bustamante and A.C. Vincent, *The Future of High-Energy Astrophysical Neutrino Flavor Measurements*, *JCAP* **04** (2021) 054 [[2012.12893](#)].
- [23] K. Riabtsev and S. Troitsky, *Energy-dependent flavor ratios, cascade/track spectrum tension and high-energy neutrinos from magnetospheres of supermassive black holes*, *Phys. Lett. B* **839** (2023) 137758 [[2204.09339](#)].
- [24] C.A. Argüelles, M. Bustamante, D.F.G. Fiorillo, Q. Liu, N. Song and A.C. Vincent, *Energy-dependent flavor ratios of High-energy Astrophysical Neutrinos*, *PoS ICRC2023* (2023) 1182.
- [25] F. Testagrossa, D.F.G. Fiorillo and M. Bustamante, *Two-detector flavor sensitivity to ultra-high-energy cosmic neutrinos*, [2310.12215](#).

- [26] M. Ahlers, K. Helbing and C. Pérez de los Heros, *Probing Particle Physics with IceCube*, *Eur. Phys. J. C* **78** (2018) 924 [[1806.05696](#)].
- [27] BAIKAL-GVD collaboration, *Diffuse neutrino flux measurements with the Baikal-GVD neutrino telescope*, *PoS ICRC2023* (2023) 1015.
- [28] KM3NeT collaboration, *Astronomy potential of KM3NeT/ARCA230*, *PoS ICRC2023* (2023) 1075.
- [29] SUPER-KAMIOKANDE collaboration, *Atmospheric neutrino oscillation analysis with external constraints in Super-Kamiokande I-IV*, *Phys. Rev. D* **97** (2018) 072001 [[1710.09126](#)].
- [30] SNO collaboration, *Direct evidence for neutrino flavor transformation from neutral current interactions in the Sudbury Neutrino Observatory*, *Phys. Rev. Lett.* **89** (2002) 011301 [[nucl-ex/0204008](#)].
- [31] DAYA BAY collaboration, *Observation of electron-antineutrino disappearance at Daya Bay*, *Phys. Rev. Lett.* **108** (2012) 171803 [[1203.1669](#)].
- [32] ICECUBE collaboration, *Flavor Ratio of Astrophysical Neutrinos above 35 TeV in IceCube*, *Phys. Rev. Lett.* **114** (2015) 171102 [[1502.03376](#)].
- [33] T. Ohlsson, *Status of non-standard neutrino interactions*, *Rept. Prog. Phys.* **76** (2013) 044201 [[1209.2710](#)].
- [34] R. Enberg, M.H. Reno and I. Sarcevic, *High energy neutrinos from charm in astrophysical sources*, *Phys. Rev. D* **79** (2009) 053006 [[0808.2807](#)].
- [35] J.A. Carpio, K. Murase, M.H. Reno, I. Sarcevic and A. Stasto, *Charm contribution to ultrahigh-energy neutrinos from newborn magnetars*, *Phys. Rev. D* **102** (2020) 103001 [[2007.07945](#)].
- [36] A. Fedynitch, R. Engel, T.K. Gaisser, F. Riehn and T. Stanev, *Calculation of conventional and prompt lepton fluxes at very high energy*, *EPJ Web Conf.* **99** (2015) 08001 [[1503.00544](#)].
- [37] S. Razzaque, P. Meszaros and E. Waxman, *TeV neutrinos from core collapse supernovae and hypernovae*, *Phys. Rev. Lett.* **93** (2004) 181101 [[astro-ph/0407064](#)].
- [38] S. Razzaque, P. Meszaros and E. Waxman, *High energy neutrinos from a slow jet model of core collapse supernovae*, *Mod. Phys. Lett. A* **20** (2005) 2351 [[astro-ph/0509729](#)].
- [39] S. Ando and J.F. Beacom, *Revealing the supernova-gamma-ray burst connection with TeV neutrinos*, *Phys. Rev. Lett.* **95** (2005) 061103 [[astro-ph/0502521](#)].
- [40] E. Waxman and J.N. Bahcall, *High-energy neutrinos from cosmological gamma-ray burst fireballs*, *Phys. Rev. Lett.* **78** (1997) 2292 [[astro-ph/9701231](#)].
- [41] K. Murase and K. Ioka, *TeV–PeV Neutrinos from Low-Power Gamma-Ray Burst Jets inside Stars*, *Phys. Rev. Lett.* **111** (2013) 121102 [[1306.2274](#)].
- [42] N. Valtonen-Mattila and E. O’Sullivan, *Prospects for Extending the Core-collapse Supernova Detection Horizon Using High-energy Neutrinos*, *Astrophys. J.* **945** (2023) 98 [[2206.00450](#)].
- [43] L. Pasquali and M.H. Reno, *Tau-neutrino fluxes from atmospheric charm*, *Phys. Rev. D* **59** (1999) 093003 [[hep-ph/9811268](#)].
- [44] A. Bhattacharya, R. Enberg, Y.S. Jeong, C.S. Kim, M.H. Reno, I. Sarcevic et al., *Prompt atmospheric neutrino fluxes: perturbative QCD models and nuclear effects*, *JHEP* **11** (2016) 167 [[1607.00193](#)].
- [45] T.K. Gaisser, *Spectrum of cosmic-ray nucleons, kaon production, and the atmospheric muon charge ratio*, *Astropart. Phys.* **35** (2012) 801 [[1111.6675](#)].

- [46] F. Riehn, H.P. Dembinski, R. Engel, A. Fedynitch, T.K. Gaisser and T. Stanev, *The hadronic interaction model SIBYLL 2.3c and Feynman scaling*, *PoS ICRC2017* (2018) 301 [[1709.07227](#)].
- [47] A.D. Martin, M.G. Ryskin and A.M. Stasto, *Prompt neutrinos from atmospheric $c\bar{c}$ and $b\bar{b}$ production and the gluon at very small x* , *Acta Phys. Polon. B* **34** (2003) 3273 [[hep-ph/0302140](#)].
- [48] M. Wallraff and C. Wiebusch, *Calculation of oscillation probabilities of atmospheric neutrinos using nuCraft*, *Comput. Phys. Commun.* **197** (2015) 185 [[1409.1387](#)].
- [49] K. Greisen, *End to the cosmic ray spectrum?*, *Phys. Rev. Lett.* **16** (1966) 748.
- [50] G.T. Zatsepin and V.A. Kuzmin, *Upper limit of the spectrum of cosmic rays*, *JETP Lett.* **4** (1966) 78.
- [51] V.S. Berezinsky and G.T. Zatsepin, *Cosmic rays at ultrahigh-energies (neutrino?)*, *Phys. Lett. B* **28** (1969) 423.
- [52] F.W. Stecker, *Diffuse Fluxes of Cosmic High-Energy Neutrinos*, *Astrophys. J.* **228** (1979) 919.
- [53] C.T. Hill and D.N. Schramm, *The Ultrahigh-Energy Cosmic Ray Spectrum*, *Phys. Rev. D* **31** (1985) 564.
- [54] S. Yoshida and M. Teshima, *Energy spectrum of ultrahigh-energy cosmic rays with extragalactic origin*, *Prog. Theor. Phys.* **89** (1993) 833.
- [55] R. Engel, D. Seckel and T. Stanev, *Neutrinos from propagation of ultrahigh-energy protons*, *Phys. Rev. D* **64** (2001) 093010 [[astro-ph/0101216](#)].
- [56] K. Kotera, D. Allard and A.V. Olinto, *Cosmogenic Neutrinos: parameter space and detectability from PeV to ZeV*, *JCAP* **10** (2010) 013 [[1009.1382](#)].
- [57] M. Ahlers and F. Halzen, *Minimal Cosmogenic Neutrinos*, *Phys. Rev. D* **86** (2012) 083010 [[1208.4181](#)].
- [58] J. Heinze, D. Boncioli, M. Bustamante and W. Winter, *Cosmogenic Neutrinos Challenge the Cosmic Ray Proton Dip Model*, *Astrophys. J.* **825** (2016) 122 [[1512.05988](#)].
- [59] R. Alves Batista, R.M. de Almeida, B. Lago and K. Kotera, *Cosmogenic photon and neutrino fluxes in the Auger era*, *JCAP* **01** (2019) 002 [[1806.10879](#)].
- [60] J. Heinze, A. Fedynitch, D. Boncioli and W. Winter, *A new view on Auger data and cosmogenic neutrinos in light of different nuclear disintegration and air-shower models*, *Astrophys. J.* **873** (2019) 88 [[1901.03338](#)].
- [61] V.P. Goncalves and M.V.T. Machado, *Saturation Physics in Ultra High Energy Cosmic Rays: Heavy Quark Production*, *JHEP* **04** (2007) 028 [[hep-ph/0607125](#)].
- [62] A. Esmaili and P.D. Serpico, *Are IceCube neutrinos unveiling PeV-scale decaying dark matter?*, *JCAP* **11** (2013) 054 [[1308.1105](#)].
- [63] M. Chianese, G. Miele and S. Morisi, *Dark Matter interpretation of low energy IceCube MESE excess*, *JCAP* **01** (2017) 007 [[1610.04612](#)].
- [64] A. Bhattacharya, A. Esmaili, S. Palomares-Ruiz and I. Sarcevic, *Probing decaying heavy dark matter with the 4-year IceCube HESE data*, *JCAP* **07** (2017) 027 [[1706.05746](#)].
- [65] A. Bhattacharya, A. Esmaili, S. Palomares-Ruiz and I. Sarcevic, *Update on decaying and annihilating heavy dark matter with the 6-year IceCube HESE data*, *JCAP* **05** (2019) 051 [[1903.12623](#)].
- [66] C.W. Bauer, N.L. Rodd and B.R. Webber, *Dark matter spectra from the electroweak to the Planck scale*, *JHEP* **06** (2021) 121 [[2007.15001](#)].
- [67] PARTICLE DATA GROUP collaboration, *Review of Particle Physics*, *PTEP* **2022** (2022) 083C01.

- [68] KAMLAND collaboration, *Precision Measurement of Neutrino Oscillation Parameters with KamLAND*, *Phys. Rev. Lett.* **100** (2008) 221803 [0801.4589].
- [69] DOUBLE CHOOZ collaboration, *Indication of Reactor $\bar{\nu}_e$ Disappearance in the Double Chooz Experiment*, *Phys. Rev. Lett.* **108** (2012) 131801 [1112.6353].
- [70] RENO collaboration, *Observation of Reactor Electron Antineutrino Disappearance in the RENO Experiment*, *Phys. Rev. Lett.* **108** (2012) 191802 [1204.0626].
- [71] K2K collaboration, *Measurement of Neutrino Oscillation by the K2K Experiment*, *Phys. Rev. D* **74** (2006) 072003 [hep-ex/0606032].
- [72] MINOS+ collaboration, *Precision Constraints for Three-Flavor Neutrino Oscillations from the Full MINOS+ and MINOS Dataset*, *Phys. Rev. Lett.* **125** (2020) 131802 [2006.15208].
- [73] T2K collaboration, *Measurements of neutrino oscillation parameters from the T2K experiment using 3.6×10^{21} protons on target*, **2303.03222**.
- [74] NOVA collaboration, *First Measurement of Neutrino Oscillation Parameters using Neutrinos and Antineutrinos by NOvA*, *Phys. Rev. Lett.* **123** (2019) 151803 [1906.04907].
- [75] T2K collaboration, *Search for CP Violation in Neutrino and Antineutrino Oscillations by the T2K Experiment with 2.2×10^{21} Protons on Target*, *Phys. Rev. Lett.* **121** (2018) 171802 [1807.07891].
- [76] I. Esteban, M.C. Gonzalez-Garcia, M. Maltoni, T. Schwetz and A. Zhou, *The fate of hints: updated global analysis of three-flavor neutrino oscillations*, *JHEP* **09** (2020) 178 [2007.14792].
- [77] “Nufit webpage.” <http://www.nu-fit.org/>.
- [78] JUNO collaboration, *Sub-percent precision measurement of neutrino oscillation parameters with JUNO*, *Chin. Phys. C* **46** (2022) 123001 [2204.13249].
- [79] HYPER-KAMIOKANDE collaboration, *Hyper-Kamiokande Design Report*, **1805.04163**.
- [80] DUNE collaboration, *Deep Underground Neutrino Experiment (DUNE), Far Detector Technical Design Report, Volume I Introduction to DUNE*, *JINST* **15** (2020) T08008 [2002.02967].
- [81] P.B. Denton, M. Friend, M.D. Messier, H.A. Tanaka, S. Böser, J.a.A.B. Coelho et al., *Snowmass Neutrino Frontier: NF01 Topical Group Report on Three-Flavor Neutrino Oscillations*, **2212.00809**.
- [82] JUNO collaboration, *Neutrino Physics with JUNO*, *J. Phys. G* **43** (2016) 030401 [1507.05613].
- [83] M. Bustamante, J.F. Beacom and W. Winter, *Theoretically palatable flavor combinations of astrophysical neutrinos*, *Phys. Rev. Lett.* **115** (2015) 161302 [1506.02645].
- [84] A. Cooper-Sarkar, P. Mertsch and S. Sarkar, *The high energy neutrino cross-section in the Standard Model and its uncertainty*, *JHEP* **08** (2011) 042 [1106.3723].
- [85] M. Ackermann et al., *High-energy and ultra-high-energy neutrinos: A Snowmass white paper*, *JHEAp* **36** (2022) 55 [2203.08096].
- [86] C. Glaser, D. García-Fernández and A. Nelles, *Prospects for neutrino-flavor physics with in-ice radio detectors*, *PoS ICRC2021* (2021) 1231.